Printing of Highly Integrated Crossbar Junctions

*Nils Sanetra, Zoi Karipidou, René Wirtz, Nikolaus Knorr, Silvia Rosselli, Gabriele Nelles, Andreas Offenhaeusser, and Dirk Mayer**

A new process is presented that combines nanoimprint lithography and soft lithography to assemble metal–bridge–metal crossbar junctions at ambient conditions. High density top and bottom metal electrodes with half-pitches down to 50 nm are fabricated in a parallel process by means of ultraviolet nanoimprint lithography. The top electrodes are realized on top of a sacrificial layer and are embedded in a polymer matrix. The lifting of the top electrodes by dissolving the sacrificial layer in an aqueous solution results in printable electrode stamps. Crossbar arrays are noninvasively assembled with high yield by printing the top electrode stamps onto bare or modified bottom electrodes. A semiconducting and a quasi metal like conducting type of polymer are incorporated in the cross points to form metal-polymer-metal junctions. The electrical characterization of the printed junctions revealed that the functional integrity of the electrically addressed conductive polymers is conserved during the assembling process. These findings suggest that printing of electrodes represents an easy and cost effective route to highly integrated nanoscale metal-bridge-metal junctions if imprint lithography is used for electrode fabrication.

1. Introduction

Polymer electronics and organic electronics provide promising platforms to introduce novel functions not accessible by common silicon technology. Prominent examples are ultrathin and flexible photovoltaic cells, large area organic light emitting diodes, and sensors for organic or biomolecules.[1] A widely employed junction configuration in soft thin film electronics is the metal–bridge–metal sandwich which is used, for instance, as a resistive switching nonvolatile memory element.[2] For these systems it was shown early on that the involved experimental conditions like high electric fields, defects in the organic layer, and vacuum deposition of the top electrode can cause irreproducible switching processes and obscure the native electronic properties of the junction material.[3] With shrinking of feature sizes, a reduction of film thickness is accompanied by technical issues, which amplifies these problems. When the film thickness reaches molecular level, destructive effects of common metal evaporation techniques on molecular layers lead to a penetration of the molecular film and formation of metal filament based shorts.[4,5] This well known effect from molecular electronics is also likely to arise for ultrathin polymer films as well.[6,7] Furthermore, most biomolecules integrated in bio-inorganic hybrid systems are incompatible with standard lithography techniques that involve harsh process conditions, aggressive chemicals, or vacuum.

The interest in organic and polymer electronics has been growing steadily in the past years, and it is speculated that these young fields will develop fully along with progress in establishing appropriate low-cost, large area manufacturing techniques, similar to the success story of Si technology.[8] Hence, novel gentle and high resolution patterning strategies are required for structuring and assembling polymer–solid hybrid systems.

In this context, soft lithography (SL) represents an alternative to conventional lithography.[9] This non invasive technique uses flexible polymer stamps to transfer various types of materials like molecular inks or solid electrodes onto target substrates. Printing is one soft lithography technique that mediates a gentle device assembly whereby incorporation of organic and biological material is enabled. It was shown that printing of metal films allows the soft deposition of metal contacts onto molecular monolayer without filament formation.[10,11]

A promising device architecture for the realization of next generation memory and logic devices on the bases of metal–bridge–metal junctions is the crossbar latch.[12–15] It can reach high data densities at high redundancy and defect tolerance, giving optimal prerequisites for the incorporation of polymer layers and molecules into the junction.[16] With regard to printed electronics, the crossbar architecture has the benefit of high tolerance in the positioning accuracy of the top electrodes on the bottom electrodes. New electronic circuitries such as the memristor are realized in a crossbar latch.[17] Because the area of each cross point junction is simply determined by the electrode widths, the number of addressed material in a junction can be easily scaled down. Patterns far below 100 nm have been created with nanoimprint lithography

N. Sanetra, Prof. A. Offenhaeusser, Dr. D. Mayer
Peter-Grünberg-Institut
Forschungszentrum Jülich GmbH, D-52428 Jülich, Germany
JARA-Fundamentals of Future Information Technology
E-mail: Dirk.Mayer@fz-juelich.de
Z. Karipidou, Dr. R. Wirtz, Dr. N. Knorr, Dr. S. Rosselli, Dr. G. Nelles
Sony Deutschland GmbH
Materials Science Laboratory
Stuttgart Technology Center
Hedelfingerstrasse 61, D-70327 Stuttgart, Germany

DOI: 10.1002/adfm.201101925

(NIL). Since it is a parallel patterning tool NIL has the potential to achieve high throughput with low-costs. Therefore NIL has been included into the ITRS Roadmap in 2003 as next generation candidate[18] and has ever since been an inherent part of the recent ITRS Roadmaps as potential successors to optical lithography.

A process named Polymer Assisted Lift Off (PALO) has recently been presented by K. T. Shimizu et al. as a promising printing technique to rapidly form metal-molecule-metal junctions.[19,20] Originally, this technique was developed to generate and transfer electrodes in the large micrometre range. The process involves optical lithography and a liftoff in aggressive basic and acidic solutions. Here we present a modified PALO-based process that combines soft lithography and state of the art NIL. The latter allows patterning of metal films in the nanometre range by a parallel and low-cost technique. The liftoff is performed in aqueous solution to facilitate gentles processing conditions possible. Metal crossbars of various width scales (10 µm–100 nm) are assembled via printing of the top contact. The printed crossbar junctions are characterized in a two-terminal setup and are shown to be selectively electrically addressable.

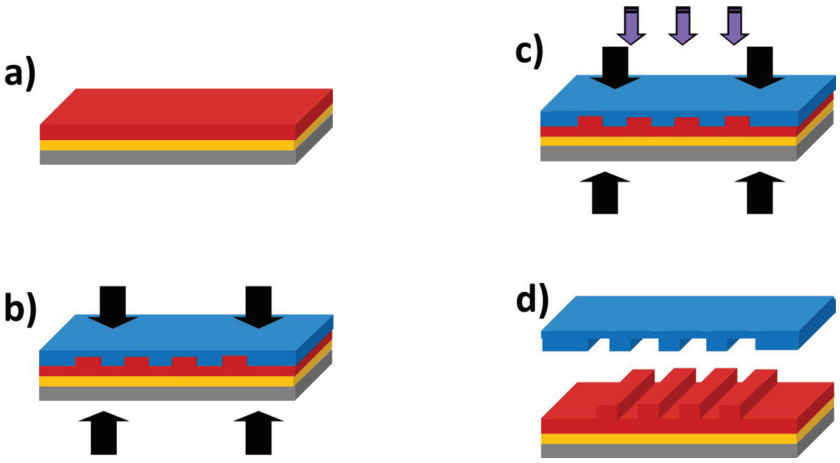

Figure 1. Electrode fabrication process with NIL. a) A gold film (yellow) on a silicon substrate with 400 nm silicon oxide (grey) is spin-coated with nanoimprint resist (red, underlayer not shown). b) The patterned UV transparent mold (blue) is pressed into the liquid resist filling out the cavities of the mold. c) the resist is cured by exposure to UV light passing through the mold. d) the mold is released from the sample with the patterned resist.

To evaluate their functionality, two types of conducting polymers (CP), the highly conducting polymers poly (3,4 ethylenedioxy-thiophene)- poly(styrenesulfonate) (PEDOT:PSS), and the semiconducting regiorandom poly(3-hexylthiophene-2,5,diyl) (P3HT), have been integrated into the crossbar junctions. Conducting polymers are widely used in various fields of research and technology due to their unique and tuneable electrical properties as well as their good processability.[21] Highly conducting polymers such as PEDOT:PSS have been used for instance as a flexible electrode material in molecular electronic junctions[22] as well as for OLEDs and LCDs.[23,24] Further applications are as anti-static coatings and as active materials in sensors.[25,26] P3HT also belongs to the class of conjugated polymers but has much lower conductivity.[27,28] Due to its p-type semiconducting properties, it is used for the development of organic photovoltaic cells. Although both polymers are considered to behave as semiconductors only PEDOT:PSS can show quasi metallic properties.[29,30] The pronounced difference in their electrical properties will be exploited to evaluate the functionality of the junctions fabricated in the scope of this work. Both conducting polymers were integrated into the printed crossbar junctions and their electrical properties were characterized by *I–V* investigations.

2. Results

A crossbar device consists of two parallel planes of wire arrays orientated perpendicular to each other. Each bar forms several cross points when crossing the wires of the other plane. The functional material incorporated into the junctions determines the overall properties of the crossbar device. Since harsh conditions during the fabrication process can destroy the functionality of the sandwiched material, a soft deposition technique is required. For the assembly of crossbar arrays by a PALO process bottom and top electrodes are fabricated on two separate substrates as described in the following sections.

2.1. Fabrication of Bottom and top Electrodes

In **Figure 1**, the NIL-based fabrication process is illustrated by way of example of the definition of the bottom electrodes. The substrate is a silicon wafer with 400 nm silicon oxide for insulation. 30 nm of gold are thermally evaporated on top of a 5 nm Ti adhesive layer. A two layer resist system is spin-coated onto the gold layer (underlayer NX-R3022 and UV-resist NX-R2010). At this stage the resist is viscously deformable, adapting to the topography of a structured imprint mold. The mold is made of a UV-transparent silicon oxide wafer with patterned depressions made by electron beam lithography (EBL). The mold surface was coated with a high quality anti-sticking layer of low surface free energy with a water contact angle of about 110°. The mold is pressed into the resist on the substrate with a pressure of typically 550 psi. The resist fills the pattern depressions of the mold and is cured by UV light exposure, transforming it into a rigid cross-linked film carrying the negative copy of the mold pattern. An inherent feature of NIL is the residual layer underneath the imprinted structures caused by excess resist. The residual layer is in general problematic and was therefore reduced to values below 40 nm by shrinking the initial layer thickness of UV resist which facilitated a high quality pattern transfer.

The whole etch process is illustrated in **Figure 2**. At first the residual layer is removed by reactive ion beam etching (RIBE) with CF_4 followed by an oxygen plasma step to etch the underlayer resist. Afterwards the pattern is transferred to a metal film by Ar sputtering. **Figure 3** shows SEM images of the final

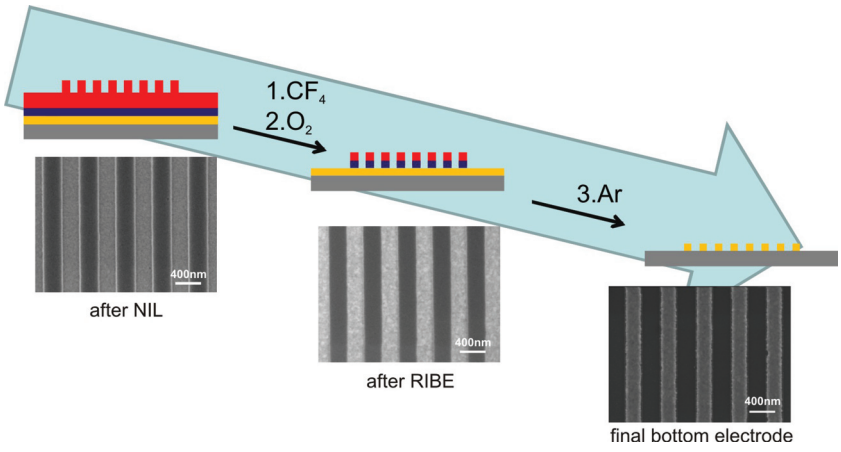

Figure 2. Scheme of the pattern transfer of the imprinted resist structures into the metal film via reactive ion beam etching. Exemplary SEM images of corresponding samples are illustrating individual process steps. The starting NIL sample is composed of a Si substrate (grey), gold film (yellow), underlayer resist (purple), and imprinted resist (red) with electrode pattern and residual layer. At first the residual layer is removed by RIBE with CF_4 and afterwards the underlayer is etched with O_2. The transfer into the metal film is carried out by sputtering with Ar.

bottom electrodes of varying widths. As reference, an image of a set of micrometer sized bottom electrodes fabricated by photolithography according to a procedure reported by Luessem et al.[17] is presented in Figure 3a. Figure 3b–d show bottom electrodes with nominal widths of 300 nm, 100 nm, and 50 nm, respectively. It should be noted that the images were recorded with almost three orders of magnitude difference in the magnification between Figure 3a and 3b, which points out the impressive patterning capabilities of nanoimprint lithography in comparison to optical lithography. In the images of Figure 3b–d the typical grain boundaries of evaporated gold films can be seen. The edge roughness of the bottom electrodes, determined by AFM, is constant for all three sizes and shows a mean root mean square (RMS) value of (4.5 ± 3.0)nm.

For the fabrication of liftable top electrodes a 300 nm water soluble sacrificial resist layer NX-R3022 is spin-coated on a silicon wafer. The new sacrificial layer features a superior mechanical stability, is insensitive electron beams to, and humidity in contrast to polyacrylic acid, used in recent PALO approaches. Subsequently, a 60 nm gold film is deposited by thermal evaporation onto this polymer layer, immediately after spin-coating. To pattern the gold film, a UV-NIL process similar to that of the bottom electrodes is carried out. For the success of the NIL process it is important that the adhesion of the gold layer to the sacrificial layer is higher than the adhesion of the mold to the UV-resist. This requirement was fulfilled for the NX-R3022 (different to polyacrylic acid) in combination with the high quality anti-sticking layer applied to the mold, since this resist was developed as adhesion promoting underlayer. The pattern of the top electrodes is defined by the transfer of the resist pattern into the metal film by reactive ion etching (RIE, same etch gases as for bottom electrodes). When etching the gold film a thin residual gold layer of 10–15 nm is left beneath the electrodes which is crucial in the following encapsulation.

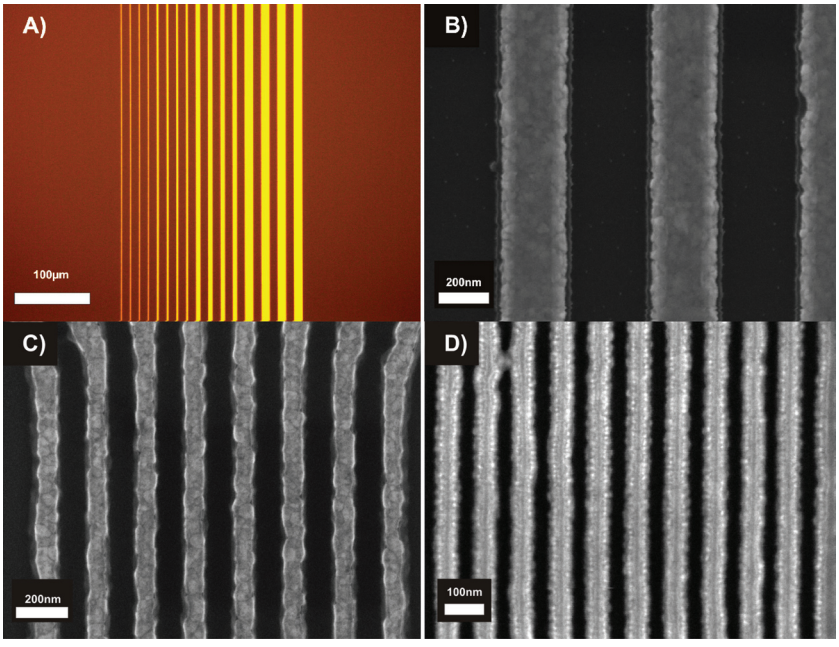

Figure 3. Images of bottom electrodes. The images show Au electrodes on a silicon/silicon oxide substrate. A) is an optical microscopy image of bottom electrodes of 1, 2, 5 and 10 µm width that have been fabricated by optical lithography according to previous reports.[18] B), C) and D) are SEM images of bottom electrodes fabricated by NIL with nominal halfpitch widths of 300 nm, 100 nm, and 50 nm, respectively. Please note the different scales of the scales bars in comparison to (A).

In the next step, a 1 µm PMMA layer is spin-coated on top of the patterned electrodes to embed the electrodes into a solid but flexible polymer matrix. The residual gold layer prevents PMMA from flowing beneath the electrodes and enclosing the electrodes completely. For better handling of the stamp structure, a several mm thick PDMS backplane is attached on top of the PMMA layer. When immersed in ultrapure deionised water (MilliQ Gradient A10, Millipore), the top electrode PMMA-PDMS stamp structure is released from the substrate wafer within a few minutes with 100% yield. In the original PALO process, the liftoff of large micrometre electrodes was performed in strongly basic and acidic solution, which increases the probability of defects if nanometre-sized electrodes are realized. The final step of the fabrication process of the top electrode structure is the removal of the residual gold layer by Ar sputtering. In our experiments it turned out to be beneficial to perform this step just before

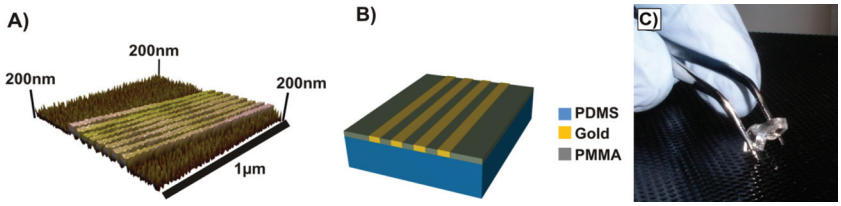

Figure 4. A) AFM topography of a top Au electrode after release and residual layer sputtering, demonstrating the protrusion of the elelctrodes. The schematic (B) depicts the structure of the top electrode: The gold electrodes are embedded in PMMA and stabilized by a PDMS backplane. C) shows a photograph of a top electrode grabbed by tweezers.

stamping the electrodes, which are cleaned from the sputtering process. In **Figure 4**a an AFM scan shows the surface corrugation of a top electrode after removal of the residual gold layer. As a result of the flexible relaxation and the thermal expansion during the removal of the residual layer, the electrodes always protrude a few nanometres out of the PMMA surrounding. This protrusion of the top electrodes is necessary to obtain electric contact to the bottom electrode in the later printing process. The layer structure of the top electrode is shown in Figure 4b.

In Figure 4c a photograph of a completed stamp with top electrodes grabbed by tweezers is shown. The PDMS backplane is flexible and the electrodes can follow the bending to some extend without taking any damage. The flexibility of the stamp structure is necessary to facilitate a conformal contact of the top electrodes to corrugations of the bottom electrodes. The surface roughness of the top electrodes as determined by AFM (data not shown) is 0.7 nm RMS on a 5 µm × 5 µm topographic scans. This roughness of the etched Au surface is comparable to the roughness for evaporated Au films.

2.2. Crossbar Assembly

Crossbar arrays were assembled by means of soft lithography namely microcontact printing (µCP) by pressing the PDMS stamp with the top electrodes onto the bottom electrode structure. The key steps of the assembly process are illustrated in **Figure 5**. Bottom and top electrodes are fabricated as described before. After lift-off and sputtering of the residual gold layer, the top electrodes are printed onto the bottom electrode structure perpendicular to each other to prepare crossbar latches. This is done with a ±5 µm lateral accuracy by mounting the bottom and top electrodes in an optical aligner (Fineplacer device). The printing process was carried out at room temperature and ambient conditions. The flexible backplane of the top electrode mediates a homogeneous and conformal contact by adapting to the corrugations of the substrate while conserving the general shape of the stamp. After the crossbar is assembled the PDMS backplane can be peeled off to enable, e.g., SEM investigations. Images of the final crossbar devices are shown in **Figure 6**. The SEM images of the electrodes were recorded with the electron beam penetrating the PMMA back plane and appear therefore slightly blurred. A microscope image of a crossbar array fabricated according to[20] is shown in Figure 6a for comparison. While Figure 6b displays a crossbar with bottom and top electrodes of identical width, in Figure 6c a crossbar with different bottom and top electrode widths is shown. Noteworthy, Figure 6c and 6b were recorded with two orders of magnitude higher magnification than Figure 6a. Since the integration density scales with the area (square of the length), this example demonstrates the superior patterning resolution of nanoimprint lithography in comparison to photolithography which results in a four orders of magnitude higher junction density. In other words the whole junctions array of 64 junction of the 100 nm crossbar sample covers a similar area as the smallest junctions point shown in Figure 6a. Furthermore, a reduced junction size supposes to be beneficial for the durability and reliability of the metal–film–metal sandwich since the total number of defects in a homogenously applied film scales with the junction area.

To evaluate the functionality of the crossbar devices two types of conducting polymers, the highly conducting PEDOT:PSS and the p-type semiconducting P3HT, were incorporated into the crossbar junctions. Thin films in the range of 40–120 nm thickness of the conducting polymer were obtained via spin-coating onto the bottom electrodes at different spin velocities and using varying dilutions of the polymers The cross sections of PEDOT:PSS films covering a gold pad, and several bottom electrodes are presented in **Figure 7**a and Figure 7b, respectively. The films are smooth and homogeneous over large areas and adapt to surface corrugations generated by the electrode structures. The Au–polymer–Au junctions were assembled by printing a top electrode onto a polymer coated bottom electrode.

2.3. Electrical Characterisation

All devices examined in the following have been assembled by the printing technique described above and are electrically

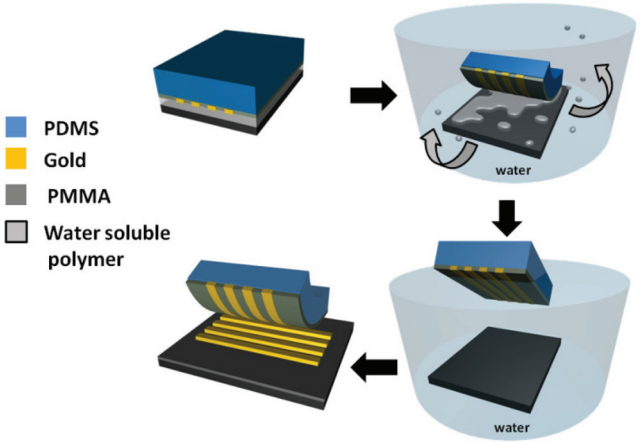

Figure 5. Schematic of the PALO process: electrodes are defined by NIL on a water soluble layer and stabilized with a PDMS backplane. When immersed in water the top electrodes releases from substrate. The PDMS backplane makes the electrode easy to handle and mediates conformal contact by its flexibility when printed on rigid substrate. A crossbar array is assembled by printing the top electrode perpendicular to a bottom electrode array.

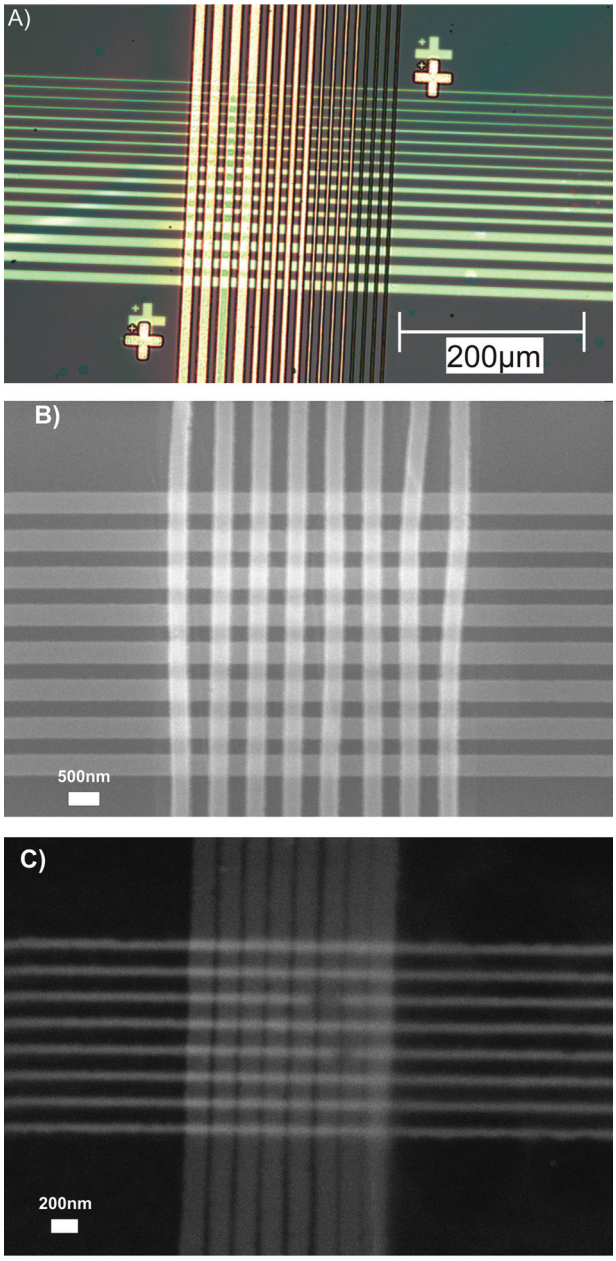

Figure 6. Images of finished crossbar arrays. A) is a microscope image and shows a crossbar fabricated by a PALO process based on optical lithography according to a previous study[18] with nominal junction areas of 1–10 µm × 1–10 µm. B) and C) show SEM images of nano-crossbar arrays fabricated by NIL combined with printing. The nominal junction size is 300 nm × 300 nm, and 100 nm × 100 nm respectively. Please note the different scales of the scales bars in (B) and (C) in comparison to A).

addressable. In a two-terminal setup, current-voltage (*I–V*) curves were recorded to characterize the devices. Nearly all of the printed crossbars (>80%) were electrically functional and in a functional device all 64 junctions showed electrical contact. The main reason for occurrence of non-functional devices was unfavourable mechanical stress on the polymer stamp during the assembling process. No data filtering was applied. The

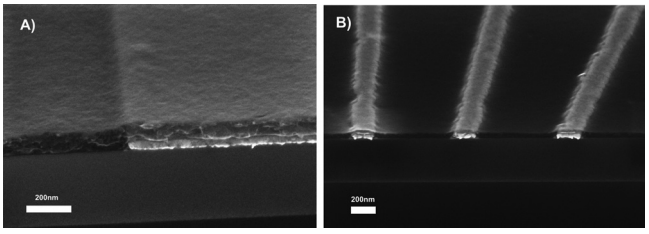

Figure 7. Cross sectional SEM images of spin coated PEDOT:PSS covering gold bottom electrodes. The thickness of the polymer layer is 120 nm and 55 nm for (A) and (B) respectively. Images were taken at an inclination angle of 60°.

uncovered bottom electrodes have a resistance of 2500, 3200, and 4300 Ω for width of 300, 200, and 100 nm respectively. Crossbars assembled from bare gold electrodes showed linear *I–V* characteristics with resistance similar to the bottom electrode resistances, signifying a good electrical contact of the top and the bottom electrodes. The data implies that the contact resistance of printed Au–Au contacts is small in comparison to the feedline resistance. The electrical characterisation of the metal–polymer–metal crossjunctions revealed that the junction currents were reduced by more than an order of magnitude in comparison to polymer free junctions, as shown in **Figure 8**a for PEDOT:PSS. The PEDOT:PSS junctions showed slightly s-shaped *I–V* behaviour similar to earlier reported results of other groups.[28,29] Since the *I–V* characteristic is almost linear and only slightly s-shaped, the contact between PEDOT:PSS and Au is considered to be ohmic in first-order approximation. Hence the junction resistance was derived by linear least square regression fits of the linear regime of the recorded *I–V* curves. Additionally, the above mentioned resistance of the bare electrodes was subtracted as feed line resistance. The employed model assumes that only the conductivity of the bulk material in the junction and not the contact resistances contributes to the junction resistance. According to this model an average value for the material conductivity of 5.7 ± 4.9 S/cm was derived for PEDOT:PSS, calculated from 11 different devices including about 200 junctions. The determined conductivity agrees reasonably well with the value of 10 S/cm specified in the data sheet of the producer,[30] and thus supports our assumption of comparable low contact resistances. The high error value reflects the fluctuations between different devices. Although single devices were very stable and no degradation in the *I–V* curves was found the current varied notably from device to device. Since the samples were prepared under similar conditions and parameters, we attribute the variations in the currents to variations in the conformity of the top electrode contacts as well as to the intrinsic properties of PEDOT:PSS. Humidity and heating of the sample can influence the polymer behaviour as well.[27] Additionally, the conductivity of PEDOT:PSS can vary locally due to inhomogeneities in the domain structure of the polymer film, which is of increasing importance when junction size is scaled down.[28]

For P3HT film junctions, s-shaped *I–V* characteristic were repeatedly observed, as a result of a non-ohmic Schottky-type contact between P3HT and Au. A pronounced s-shape can be expected for a metal–semiconductor–metal stack with two

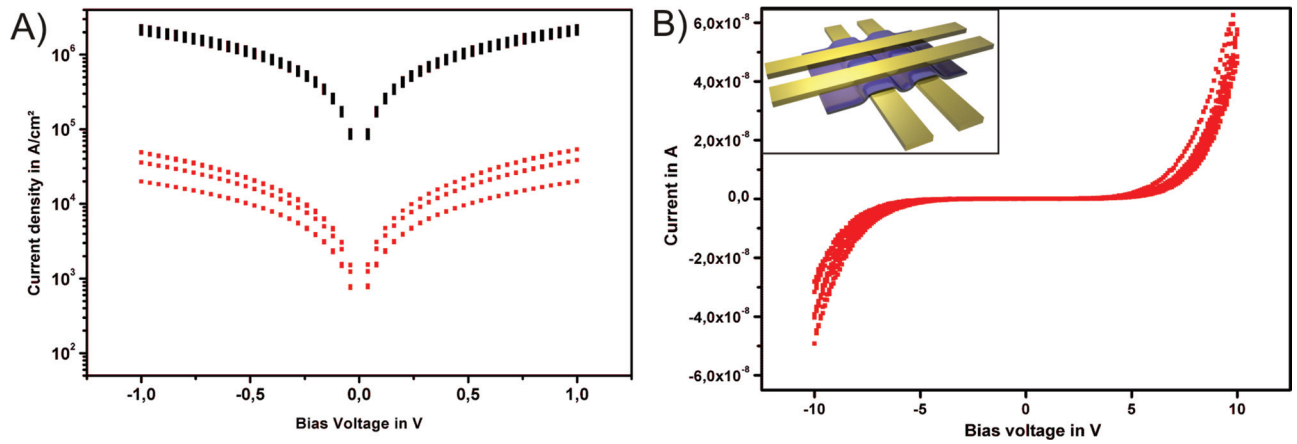

Figure 8. A) shows a semi-logarithmic plot of *J–V* measurements of crossbar junction of direct top-bottom electrode contacts (black squares) and of Au-PEDOT:PSS-Au junctions (red squares). B) shows s-shaped exemplary *I–V* curves of Au-P3HT-Au junctions measured in the same crossbar junction architecture as (A).

Schottky barriers in series. Exemplary *I–V* curves are presented in Figure 8b. The junctions were stable up to a bias of 10 V. It was not possible to estimate unambiguously the conductivity of the P3HT films due to the high resistance of the Schottky type barriers at the metal/polymer interface.

The scaling of the currents with respect to the junction area was evaluated from printed Au-PEDOT:PSS-Au junctions. Therefore, the currents at 1 V bias of the NIL crossbar junctions were compared to the currents of larger area junctions fabricated by photolithography and shadow mask evaporation. All junctions contained PEDOT:PSS of equal type and layer thickness. Plotting the junction current versus the junction area (black dots in **Figure 9**) in a double logarithmic graph results in a square root dependence. A linear dependence between current and area would be expected if the junction resistance is the main contributor to the resistance. The square root dependence is a result of the growing influence of the feed line resistance on the junction resistance for small junction areas, i.e., the current scales with the width of the lines rather than the area of the junction as the main resistance contribution stems from the long and thin feed lines rather than the actual junction.

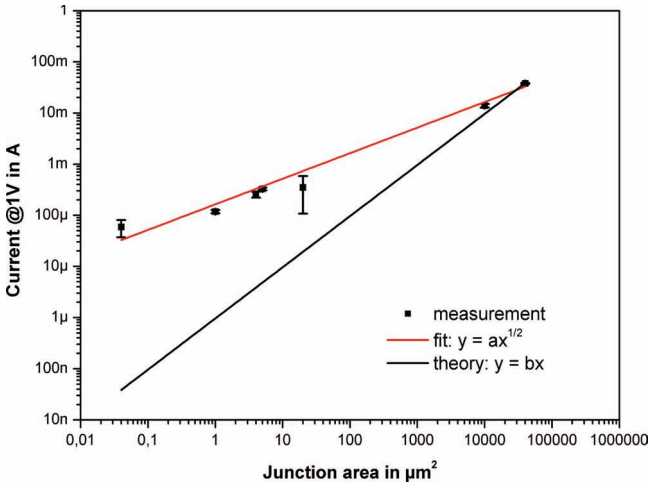

Figure 9. Dependence of the junction currents on the junction area: A linear dependence between current and area would be expected if the junction resistance is the main contributor to the resistance. The square root dependence, however, indicates that the long feed-lines have a greater contribution than the junction itself.

3. Conclusions

In summary we have successfully combined the fabrication of nanoscale metal electrodes by ultraviolet nanoimprint lithography with a soft printing process to assemble highly integrated crossbar arrays. Therefore, the original PALO process was redesigned to adapt to high performance nanoimprint lithography. The combined NIL/PALO process facilitates a parallel fabrications of nanometre sized metal electrodes and a gentle, high yield printing of them into crossbar arrays. The 10 to 100 times smaller feature sizes of the electrodes in comparison to electrodes fabricated by optical lithography provide up to four orders of magnitude higher integration density in the final crossbar arrays.

To demonstrate the suitability of this new PALO process we assembled crossbar junctions in the nanometer range. Therefore, top electrodes were fabricated on a liftable polymer stamp by means of UV-NIL. Metal crossbars with varying electrode size of 8 bit × 8 bit and junction areas down to 100 nm × 100 nm were printed and electrically addressed. Furthermore, the functionality of the devices was demonstrated by integrating and electrical characterization of two conducting polymers PEDOT:PSS and P3HT showing quasi metal and semiconductor behaviour, respectively. For PEDOT:PSS a conductivity value of (5.7 ± 4.9) S/cm was measured that agrees with the material specifications. In this work we have demonstrated in proof of principle experiments that printed crossbar arrays are a suitable framework for the incorporation and electrical investigation of organic materials into metal-film-metal junctions. Furthermore, it can be envisioned to alter the electrical properties of the junction by using electrode materials of different work functions. Also the incorporation of proteins or bistable organic materials could lead the way to new applications.

4. Experimental Section

The fabrication processes were carried out in level 10 and level 100 clean rooms with controlled humidity and temperature. Silicon and silicon oxide wafers were purchased from the company Si-Mat. Aqueous solutions were prepared with 18 Ω cm deionized water (Millipore MilliQ Gradient A10). PEDOT:PSS was purchased from H. C. Starck (Clevios P) and diluted in methanol. Regiorandom P3HT (Rieke Metals, Inc) was dissolved in toluene. All other chemicals were purchased from Sigma Aldrich and used as received. Electrodes were printed with a fine-placer from Finetec.

Nanoimprint Mold Fabrication: The NIL mold was made out of SiO_2 and the pattern was defined by electron beam lithography (EBL). 10 nm of Cr were deposited (Pfeifer PLS 500 evaporation chamber from Oxford Inst.) on the insulating SiO_2 wafer (Crystec GmbH) as a conducting layer to compensate surface charging effects. A polymethylmethacrylat (PMMA AR-P 649.04, Allresist) film was spin coated at 4000 rpm resulting in a layer thickness of approx. 140 nm. The pattern of parallel bars with feed lines for electrical connection was written with a Leica EBPG 5HR electron beam writer and developed afterwards (developer AR-P 600-55, Allresist). The nominal half-pitch size of the bars was 300, 200, 100, and 50 nm. Next the pattern was transferred into the Cr layer by Ar sputtering in a reactive ion beam etching (RIBE) device (ionfab300plus from Oxford Ins.). This Cr layer served as a hard mask for the following etching of the SiO_2 by RIBE with CF_4. Finally, the Cr mask was removed in a wet etch solution (ceric ammonium nitrate: perchloric acid: H_2O, 10.9%: 4,25%: 84,85%, from Microchemicals). The mold was coated with 1*H*,1*H*,2*H*,2*H*-perfluorodecyltrichlorosilane as an anti-sticking layer. A monolayer was obtained by in situ deposition from the gas phase after surface activation by oxygen plasma treatment. The silanization process was carried out in a self-made device that allows precise control of atmosphere, pressure, and temperature. The quality of the SAM was evaluated by measuring the water contact angle (OCA device from DataPhysics).

Nanoimprint: NIL was performed in a Nanonex 2000 imprint device from Nanonex Corp. The resist NX-R2010 (solid content 3%) and NX-R3022 (solid content 1.5% and 6%) were also purchased from Nanonex Corp. The UV-resist NX-R2010 was diluted in methyl metacrylat (ratio 1:1) and NX-R3022 was used as received. Parameters of the NIL process are as follows: process time 6 min, process pressure 550 PSI, exposure time 4 min, room temperature.

Polymer Film Deposition: PEDOT:PSS films were spincoated with a WS-400E-NPP-Lite spincoater from Laurell. Spin velocities ranged from 2000–7000 rpm. After spincoating the films were baked at 150 °C on a hotplate in air for 2 min. P3HT was spincoating at 2000 rpm for 60s and baked over night at 100 °C in a vacuum oven.

Characterization: Scanning electron microcope images were obtained with a Gemini 1550 from Zeiss. For all images the InLense detector and an acceleration voltage between 10 and 20 keV were used. Atomic force microscope images were taken with a Nanoscope IV Multimode (Veeco Instruments, USA) in tapping mode with a silicon cantilever (RTESPW f_0 = 232–294 kHz, Veeco Instruments). Electrical measurements were performed with a Semiconductor Characterization System (SCS) 4200 from Keithly (including Capacity Voltage (CV) Analyser 590 and CV meter 595).

Acknowledgements

René Borowski and Michael Prömpers are kindly acknowledged for their technical support during the development of the fabrication process. Furthermore, we thank Hans Wingens for the deposition of different metal layers in the clean room. We also acknowledge Dr. Stephan Trellenkamp for ebeam writing.

Received: August 16, 2011
Revised: October 19, 2011
Published online: January 10, 2012

[1] D. R. Paul, L. M. Robeson, *Polymer* **2008**, *49*, 3187.
[2] J. C. Scott, L. D. Bozano, *Adv. Mater.* **2007**, *19*, 1452.
[3] M. M. Maitani, T. A. Daniel, O. M. Cabarcos, D. L. Allara, *J. Am. Chem. Soc.* **2009**, *131*, 8016.
[4] C. R. Hansen, T. J. Soerensen, M. Glyvradal, J. Larsen, S. H. Eisenhardt, T. Björnholm, M. M. Nielsen, R. Feidenhansl, B. W. Laursen, *Nano Lett.* **2009**, *9*, 1052.
[5] L. Kunardi, C. Troadec, N. Chandrasekhar, *J. Chem. Phys.* **2005**, *123*.
[6] M. Baibarac, P. Gomez-Romero, *J. Nanosci. Nanotechnol.* **2006**, *6*, 289.
[7] E. Menard, M. A. Meitl, Y. G. Sun, J. U. Park, D. J. L. Shir, Y. S. Nam, S. Jeon, J. A. Rogers, *Chem. Rev.* **2007**, *107*, 1117.
[8] Y. N. Xia, G. M. Whitesides, *Ann. Rev. Mater. Sci.* **1998**, *28*, 153.
[9] Y. L. Loo, D. V. Lang, J. A. Rogers, J. W. P. Hsu, *Nano Lett.* **2003**, *3*, 913.
[10] J. W. P. Hsu, Y. L. Loo, D. V. Lang, J. A. Rogers, *J. Vac. Sci. Technol. B* **2003**, *21*, 1928.
[11] M. Meier, C. Schindler, S. Gilles, R. Rosezin, A. Rudiger, C. Kugeler, R. Waser, *Electron Device Lett., IEEE* **2009**, *30*, 8.
[12] J. Borghetti, Z. Y. Li, J. Straznicky, X. M. Li, D. A. A. Ohlberg, W. Wu, D. R. Stewart, R. S. Williams, *Proc. Nat. Acad. Sci. USA* **2009**, *106*, 1699.
[13] Q. F. Xia, W. Robinett, M. W. Cumbie, N. Banerjee, T. J. Cardinali, J. J. Yang, W. Wu, X. M. Li, W. M. Tong, D. B. Strukov, G. S. Snider, G. Medeiros-Ribeiro, R. S. Williams, *Nano Lett.* **2009**, *9*, 3640.
[14] K. Asadi, M. Y. Li, N. Stingelin, P. W. M. Blom, D. M. De Leeuw, *Appl. Phys. Lett.* **2010**, *97*.
[15] G. Snider, P. Kuekes, T. Hogg, R. S. Williams, *Appl. Phys. A: Mater. Sci. Process.* **2005**, *80*, 1183.
[16] H. Schift, *J. Vacuum Sci. Technol. B* **2008**, *26*, 458.
[17] K. T. Shimizu, J. D. Tabbri, J. J. Jelincic, N. A. Melosh, *Adv. Mater.* **2006**, *18*, 1499.
[18] B. Lussem, Z. Karipidou, A. Schreiber, A. Yasuda, J. M. Wessels, G. Nelles, *Microelectron. Eng.* **2010**, *87*, 614.
[19] S. Kirchmeyer, K. Reuter, *J. Mater. Chem.* **2005**, *15*, 2077.
[20] H. B. Akkerman, P. W. M. Blom, D. M. de Leeuw, B. de Boer, *Nature* **2006**, *441*, 69.
[21] M. Boussoualem, R. C. Y. King, J. F. Brun, B. Duponchel, M. Ismaili, F. Roussel, *J. Appl. Phys.* **2010**, *108*.
[22] B. Y. Qi, J. X. Luo, S. Y. Li, L. X. Xiao, W. F. Sun, Z. J. Chen, B. Qu, Q. H. Gong, *Proc. SPIE*, **2010**, *7852*, 78520.
[23] C. C. Qiu, J. K. Wang, S. M. Mao, W. H. Guo, S. J. Cheng, Y. X. Wang, *Polymers for Advanced Technologies* **2010**, *21*, 651.
[24] N. Sanetra, V. Feig, B. Wolfrum, A. Offenhausser, D. Mayer, *Phys. Status solidi C* **2011**.
[25] T. A. Chen, X. M. Wu, R. D. Rieke, *J. Am. Chem. Soc.* **1995**, *117*, 233.
[26] S. Ukai, H. Ito, K. Marumoto, S. I. Kuroda, *J. Phys. Soc. Jpn.* **2005**, *74*, 3314.
[27] A. M. Nardes, M. Kemerink, M. M. de Kok, E. Vinken, K. Maturova, R. A. J. Janssen, *Org. Electron.* **2008**, *9*, 727.
[28] H. J. Lee, J. Lee, S. M. Park, *J. Phys. Chem. B* **2010**, *114*, 2660.
[29] H. Y. Jeong, J. Y. Kim, T. H. Yoon, S. Y. Choi, *Curr. Appl. Phys.* **2010**, *10*, E46-E49.
[30] Product data sheet of Clevios P is available at the Clevios homepage at www.clevios.com/en/downloads/heraeus-conductive-polymers-downloads.aspx.